Spin glass to cluster glass transition in geometrically frustrated $CaBaFe_{4-x}Li_xO_7$ ferrimagnets

K. Vijayanandhini, Ch. Simon, V. Pralong, V. Caignaert, and B. Raveau*
CRISMAT, UMR 6508, CNRS-ENSICAEN, Université de Caen, 14050 Caen, France
(Received 4 March 2009; published 5 June 2009)

The solid solutions of $CaBaFe_{4-x}Li_xO_7$ ($CBFLi_x$) with the "114" hexagonal symmetry ($P6_3mc$) could be synthesized for $0 \leq x \leq 0.4$. The dc magnetization study of these oxides shows that they are ferrimagnetic (FiM). The FiM to paramagnetic transition temperature, T_C, decreases from 265.6 K for $x=0$ to 97.5 K for $x=0.4$ in agreement with the introduction of the diamagnetic Li^{1+} cation at the Fe sublattice. No magnetic saturation is observed and the coercive field H_C is very large, ranging from 0.7 to 0.9 T at 5 K. Importantly, the ac magnetic susceptibility, $\chi_{ac}(T)$, indicates a frequency-dependent freezing temperature, T_f, increasing with frequency and satisfying the conventional power law, $\tau/\tau_0=(T_f/T_{SG}-1)^{-z\nu}$. For the undoped $CaBaFe_4O_7$ (CBFO) ($x=0$), the best fitting parameters are characteristic of a spin glass with a transition temperature $T_{SG}=176$ K, spin-relaxation time $\tau_0=4.9\times10^{-12}$ s, and critical exponent ($z\nu$) of 6.4. In contrast, for $CBFLi_x$ ($0.1 \leq x \leq 0.4$) series the τ_0 increases from 1.3×10^{-14} to 8×10^{-16} s as x is increased; the values of $z\nu$ are in the range of 12–13, which lies much closer to that of cluster glasses ($\tau_0=10^{-14}-10^{-16}$ sec; $z\nu=12-14$). The resistivity behavior is consistent with small polaronic hopping which changes to variable range hopping at low temperatures. The measurements under $H\sim7$ T show that only CBFO (undoped) exhibits magnetoresistance, with a maximum value of 4.3% at 264 K.

DOI: 10.1103/PhysRevB.79.224407 PACS number(s): 75.50.Lk

I. INTRODUCTION

There have been a great number of studies on the magnetic frustration in oxides, such as pyrochlores[1] or spinels,[2,3] due to the peculiar triangular geometry of the framework of these compounds. In this respect, the recently discovered "114" cobaltites, $LnBaCo_4O_7$ family with Ln=lanthanide or yttrium,[4,5] have raised considerable interest. These compounds are reported to exhibit a structural transition whose characteristic temperature (T_s) increases as the ionic radius of the Ln^{3+} cation is decreased.[6] For instance, T_s increases from 160 K for Yb^{3+} (Ref. 7) up to 300 K for $Ln=Y^{3+}$,[8] through $T_s=220$ K for $Ln=(Yb_{0.5}Y_{0.5})^{3+}$.[9] This structural phase transition is characterized by a magnetostriction effect revealed by the abrupt change in crystal symmetry from hexagonal (space group $P3_1c$) (at $T>T_s$) to orthorhombic (space group $Pbn2_1$) at ($T<T_s$) transition.[10] Interestingly, this structural transition is associated with a release of a geometric frustration below T_s, giving rise to short-range antiferromagnetic (AFM) interactions and finally to a three-dimensional (3D) long-range AFM ordering. Such properties of $LnBaCo_4O_7$ are strongly correlated with its unique structure which consists of 1:1 ordered stacking of triangular and kagome layers of CoO_4 tetrahedra. There exist a number of reports on the substituted cobaltites such as $LnBa(Co,M)O_7$ ($M=Ni^{3+}$, Zn^{2+}, etc.),[11,12] whose magnetic properties also reflected more or less like frustrated magnetic structure.

Recently, a series of mixed valent 114 ferrites, $Ca_{1-x}Y_xBaFe_4O_7$, was reported[13,14] with structures closely related to that of hexagonal cobaltites and also cubic spinel and hexagonal ferrites. They are described as the stacking of close-packed $[BaO_3]_\infty$ and $[O_4]_\infty$ layers whose tetrahedral cavities are occupied by Fe^{2+}/Fe^{3+} species, forming triangular and kagome layers of FeO_4 tetrahedra. The magnetization studies of these compounds emphasize their unique behavior, ranging from ferrimagnetic for hexagonal $CaBaFe_4O_7$ (CBFO) with a T_C of 270 K, to a spin glass for cubic $YBaFe_4O_7$ and suggest a possible magnetic frustration in the ferrimagnetic compounds. In order to understand the magnetic frustration in these systems, we have attempted to synthesize a series of $CaBaFe_{4-x}Li_xO_7$ ($CBFLi_x$) ferrites and investigate in detail the modified transport and magnetic properties from that of the undoped CBFO. The chosen diamagnetic substituent (Li^{1+}) at the Fe sublattice does not carry any magnetic moment and is not expected to participate in the ferrimagnetic (FiM) interaction. Furthermore, the Li^{1+} substituent only dilutes the magnetic sublattice. Therefore, the goal of the present work is to address in more detail the diamagnetic substitutional effects on the static and dynamic magnetic properties of $CaBaFe_{4-x}Li_xO_7$ by combined measurements of ac and dc magnetic susceptibilities. Detailed measurements were performed on the real $\chi'_{ac}(T)$ and imaginary $\chi''_{ac}(T)$ components of the magnetic susceptibilities, under different driving ac magnetic-field frequencies (f) focusing mainly on the H_{ac} and frequency dependences. Systematic correlations have been brought between the nature of substituting ion and the substitution-induced spin glass to cluster glasslike transition in $CaBaFe_{4-x}Li_xO_7$.

II. EXPERIMENTAL DETAILS

Phase-pure samples of $CaBaFe_{4-x}Li_xO_7$ (referred to as $CBFLi_x$) were prepared by solid-state reaction technique. The compounds $CaBaFe_{4-x}Li_xO_7$ were prepared in two steps: first a mixture of CaO (99.96%, Fluka), Li_2CO_3 (99.98%), $BaCO_3$ (99.96%), and Fe_2O_3 (99.98%) (all chemicals from Merck) in the required molar ratio was heated in air at 873 K (12 h) for decarbonation, and in a second step the adequate amount of metallic iron was added in order to satisfy the formula, $CaBaFe_{4-x}Li_xO_7$. The decarbonated powders were calcined at ~1173 K (48 h). The granulated powder was then pressed into rectangular bars under 200 MPa. The green

bars were disposed in an aluminum-oxide finger and sealed in silica tubes under vacuum and sintered at $T_{sinter} \sim 1273$ K (24 h) and cooled at the rate of 120 K/hr. The sintered ceramic bars were postsinter annealed in sealed tubes for extended periods of 30–48 h at $T_{anneal} < T_{sinter}$ in order to improve the oxygen homogeneity. The phase purity of $CBFLi_x$ samples was ascertained by x-ray powder diffraction (XRPD). The chemical analysis of the sample using cerimetric titration shows that the oxygen stoichiometry is "$O_{7.02\pm0.02}$". The energy dispersive spectroscopy (EDS) and atomic absorption spectroscopy (AAS) analyses confirm that the cationic compositions are in good agreement with the nominale ones within the limit of the experimental errors.

The XRPD pattern was registered with a Panalytical X'Pert Pro diffractometer having the nickel-filtered Cu-$K\alpha$ source under a continuous scanning method in the 2θ range of 5–120° and step size of $\Delta 2\theta = 0.0167°$. A Rietveld analysis of XRPD data was carried out with the FULLPROF refinement program.[15] Ohmic contacts were provided to the sintered ceramic bars ($10 \times 2 \times 2$ mm^3) by the fired-on silver (Dupont, USA). Soldering for copper electrical leads was carried out with 60Sn/40Pb solder in order to have least contact resistance. Electrical resistivity, $\rho(T)$, was measured from 5 to 320 K using the four-probe dc technique. The magnetotransport properties were carried out using standard four-contact geometry in a physical property measurement system (PPMS) from Quantum Design. The dc magnetization (DCM) measurements were performed using a superconducting quantum interference device (SQUID) magnetometer equipped with variable-temperature cryostat (Quantum Design, San Diego, USA) (1.8–400 K; 0–5 T). The ac susceptibility, $\chi_{ac}(T)$ was measured with a PPMS from Quantum Design with the frequency ranging from 125 Hz to 10 KHz and between 5–320 K ($H_{dc}=0$ Oe and $H_{ac}=10$ Oe). All the magnetic properties were registered on the dense ceramic disks of $\sim 4 \times 2 \times 2$ mm^3 dimensions.

III. RESULTS AND DISCUSSION

A. Structural characterization of the samples

The Rietveld analysis from the XRPD data confirms the hexagonal structure (SG: $P6_3mc$) for $CBFLi_x$ series. No detectable secondary phases even as minor reflections in the XRPD patterns were discernible. The bottom curves in Figs. 1(a)–1(c) correspond to the difference between the observed and calculated diffraction patterns. Satisfactory matching of the experimental with the calculated profiles of the XRPD data (Table I) with better goodness of fit can be appreciated from the curves. The corresponding reliability factors R_F are 6.74% and $R_{Bragg}=8.66\%$ (Fig. 1) showing that the structure types of $CaBaFe_{4-x}Li_xO_7$ are very reasonably accurate. The crystal lattice parameters and the corresponding unit cell volume (V) of $CBFLi_x$ (Fig. 1) decreases linearly as the lithium content increases, in agreement with the small sizes of Li^{1+} (0.59 Å) and Fe^{3+} (0.49 Å) in tetrahedral coordination compared to Fe^{2+} (0.63 Å) according to Shannon and Prewitt.[16]

B. Evolution of the magnetization versus temperature

The temperature dependence of DCM was registered according to the standard zero-field-cooled (ZFC) (M_{ZFC}) and field-cooled (M_{FC}) procedures. In order to warrant the same initial conditions for the residual magnetic field and for the samples magnetic state, before the measurements of M_{ZFC} and M_{FC} curves, the following demagnetization protocols previously described by Wang *et al.*[17] were used. The magnetic-field strength was stepped down in magnitude and switched polarity with each step, i.e., a field of approximately −3 T was applied and lowered to zero through oscillations at $T=300$ K. Then the temperature was lowered down to 5 K, where the magnetic field of ~0.3 T was applied and the measurements were performed during the warming ramp up to 400 K. The M_{FC} curve was recorded during the heating from 5 to 400 K using the same rate. Other protocols, normally adapted for nanomagnetic arrays with frustrated interactions,[17] were also tried but did not change the results fundamentally.

In Fig. 2(a) some typical $M_{ZFC}(T)$ and $M_{FC}(T)$ curves registered with the applied field of $H_{dc} \sim 3$ kOe are pre-

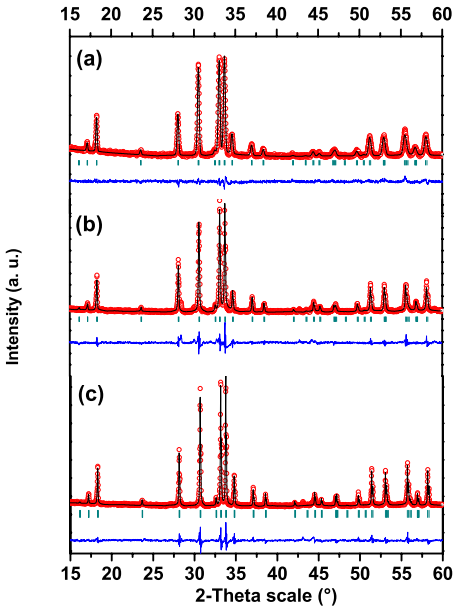

FIG. 1. (Color online) Observed x-ray diffraction intensity (○) and calculated curve (line) for (a) $CaBaFe_4O_7$, (b) $CBFLi_{0.1}$, and (c) $CBFLi_{0.4}$. The bottom curve is the difference of patterns, $y_{obs}-y_{cal}$, and the small bars indicate the angular positions of the allowed Bragg reflections.

TABLE I. Refined crystal structure parameters as obtained from the Rietveld refinement of x-ray powder diffraction data.

Crystal structure parameters	$CaBaFe_4O_7$	$CaBaFe_{3.9}Li_{0.1}O_7$	$CaBaFe_{3.6}Li_{0.4}O_7$
Unit cell parameters (Å)	$a=6.35$ $b=10.355$	$a=6.345$ $b=10.340$	$a=6.338$ $b=10.307$
Crystal system	Hexagonal	Hexagonal	Hexagonal
Space group	$P6_3mc$	$P6_3mc$	$P6_3mc$
Cell volume V (Å^3)	361.6	360.51	358.62
Reliability factor (R_F) (%)	8.4	6.2	5.48

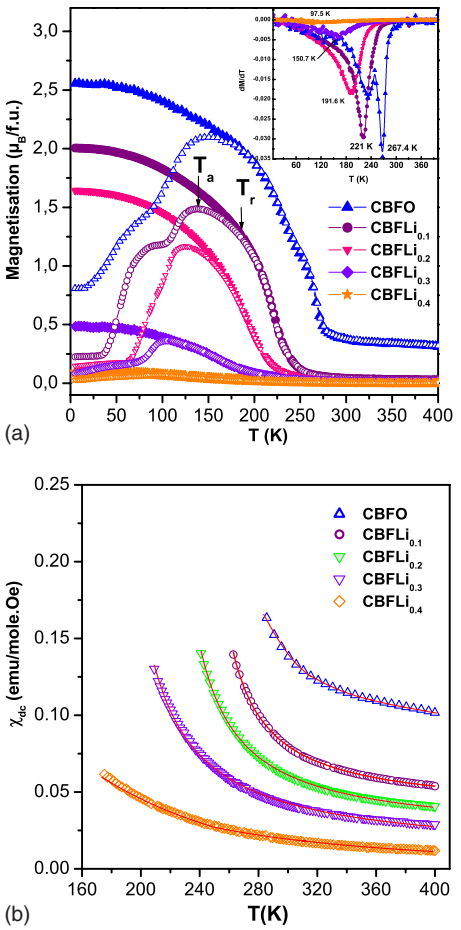

FIG. 2. (Color online) (a) Typical $M_{ZFC}(T)$ and $M_{FC}(T)$ curves of CBFLi$_x$ measured at 0.3 T. The empty symbols are for $M_{ZFC}(T)$ and the solid symbols for $M_{FC}(T)$. $M_{ZFC}(T)$ attains a maximum at temperature denoted by T_a and T_r the temperatures, where $M_{FC}(T)$ and $M_{ZFC}(T)$ start deviating. See text for details. The T_c values are indicated in the first derivative of magnetization dM/dT versus temperature (Inset). (b) Plot of the dc magnetic susceptibility (χ_{dc}) as a function of temperature, measured under $H=3$ kOe. The Open symbols and solid lines represent the experimental data and Curie-Weiss fit in the high-temperature paramagnetic region.

sented. Table II lists some of important data extracted from the DCM measurements. The saturation magnetization M_s (at 5 K) decreases slightly from $2.60\mu_B$/f.u. for the undoped samples to $2.11\mu_B$/f.u. for $x=0.1$ and then decreases drastically as the lithium content increases down to $\sim 1.15\mu_B$/f.u. for $x=0.3$. In any case, this value of the magnetization cannot be explained by true ferromagnetic or ferrimagnetic coupling at Fe site which would involve much higher theoretical (M_o). The FiM to paramagnetic (PM) transition or Curie temperatures (T_C) values were extracted from the $M_{FC}(T)$ curves, i.e., the inflection point where dM/dT is a minimum [Fig. 2(a) inset]. One observes that T_C values (Table II) decrease monotonically with increasing lithium content from 265.6 K for $x=0$ to 97.5 K for $x=0.4$. This effect is explained by the fact that the Li^{1+} ions do not carry any magnetic moment and as such they are not expected to participate in the FiM interactions; hence, the substituents only dilute the FiM coupling. Consequently, a random distribution of Fe and substituent ions in the Fe sublattice might lead to frustrated exchange interactions in these FiM solids, leading to local spin reversal and/or loss of spin collinearity. The effects mentioned above may possibly lead to the reduced M_s observed in $M(T)$ curves. The $M_{FC}(T)$ and $M_{ZFC}(T)$ curves exhibit a strong irreversibility as indicated by the appearance of large bifurcation between them at lower temperatures. M_{ZFC} curves exhibit a rather broad peak (namely, at T_a) where it attains a maximum. In Fig. 2(a), the T_r denotes the temperature where $M_{ZFC}(T)$ and $M_{FC}(T)$, at a fixed field, start merging. All the M_{FC} curves of CBFLi$_x$ continue to increase with decreasing temperature without any saturation. However, the $M_{ZFC}(T)$ and $M_{FC}(T)$ curves are substantially identical in the region, $T_r < T < T_C$ implying a reversibility of magnetization—hence, thermomagnetic irreversibility (TRM). That is, the divergence of M_{FC} and M_{ZFC} curves is observed below T_C for all CBFLi$_x$ samples with ($0 \leq x \leq 0.4$). The observation of nonsaturating magnetization values and the TRM is a common feature of FiM systems and known exotic magnetic systems such as spin glasses, cluster glasses, and superparamagnets and was also seen in randomly canted ferromagnets with perovskite structures.[18,19]

Figure 2(b) shows a plot of the dc magnetic susceptibility versus temperature $\chi_{dc}(T)$ for CBFLi$_x$ samples, measured at 5–400 K under $H=3$ kOe. Susceptibility data above 200 K fit to the Curie-Weiss law, $\chi = C/(T-\theta_{CW})$, where C and θ_{CW} are the Curie-Weiss constant and Curie temperature, respectively. The Curie-Weiss temperature is in the range of $\theta_{CW} = 236-90$ K for CBFLi$_x$ samples. The effective magnetic moment per f.u. can be expressed in Bohr magnetons (μ_B)

TABLE II. Magnetic properties of CaBaFe$_{4-x}$Li$_x$O$_7$ samples calculated from the dc magnetization data measured using SQUID magnetometer. T_c and θ_{CW} are the Critical and Curie-Weiss temperatures. μ_{eff} is the effective paramagnetic moment calculated in the PM regime of M-T data. $\mu_{H,5\ K}$ and $\mu_{H,100\ K}$ are the saturation moments at 5 and 100 K; $H_{c,5\ K}$ and $H_{c,100\ K}$ are the coercivities at 5 and 100 K, respectively.

Sample	T_C (K)	θ_{CW} (K)	μ_{eff} (μ_B/f.u.)	$\mu_{H,5\ K}$ (μ_B/f.u.)	$\mu_{H,100\ K}$ (μ_B/f.u.)	$H_{c,5\ K}$ (T)	$H_{c,100\ K}$ (T)
0	265.6	268.3	3.2(2)	2.6	2.3	0.75	0.14
0.1	221.2	236	3.75 (2)	2.11	2.09	1.24	0.69
0.2	191.6	211.9	4.37 (2)	1.36	1.4	1.17	0.21
0.3	150.7	174.1	4.97 (2)	~1.15	~0.9	0.98	0.041
0.4	97.5	90	5.55 (2)	–	–	0.36	–

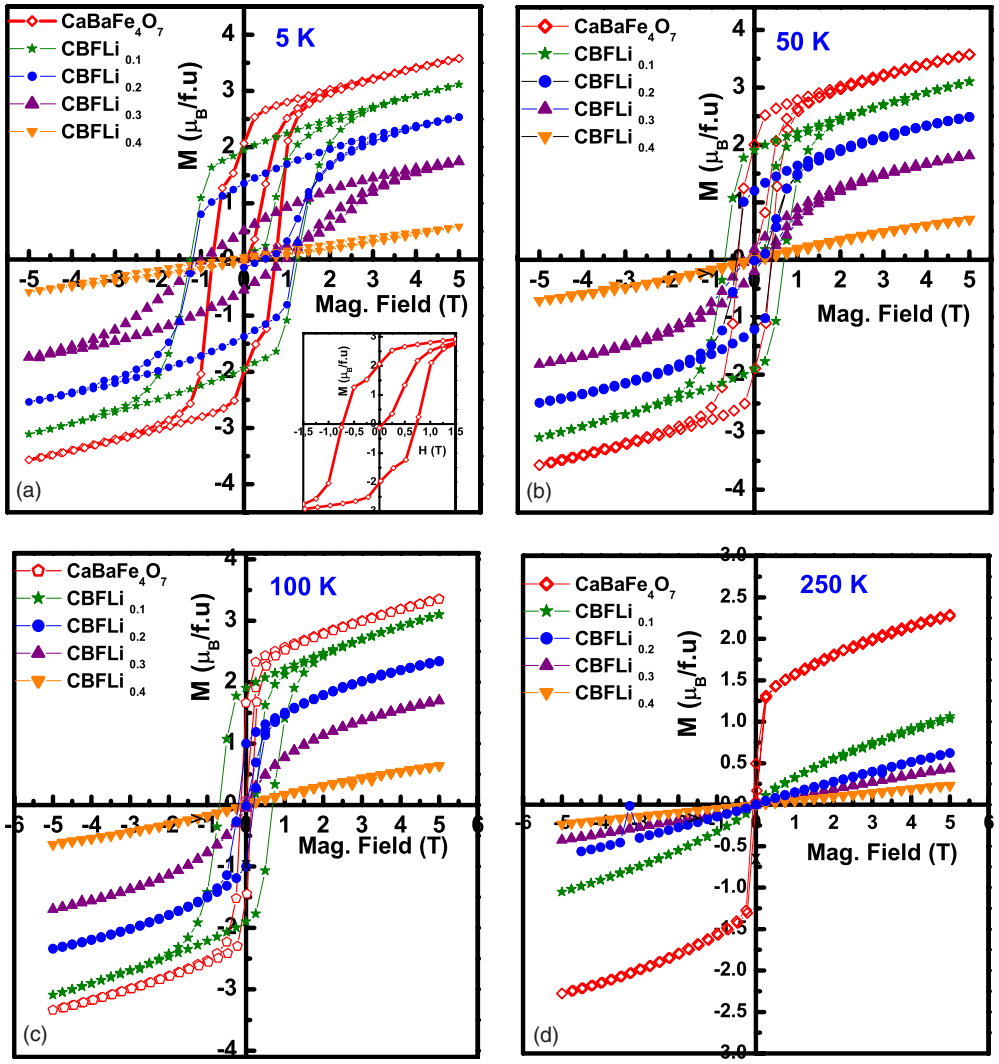

FIG. 3. (Color online) Magnetization as a function of field for all samples, measured at (a) 5, (b) 50, (c) 100, and (d) 250 K. The magnetization values are expressed in terms of μ_B/f.u.

by $\mu_{\text{eff}}=(3k_BCA/N_A)^{1/2}$, where k_B is the Boltzmann constant, A is the molecular weight, and N_A is the Avogadro number. One important point concerns the highest value of the effective magnetic moment μ_{eff} that can be reached for this compound which is only of $3.2\mu_B$/f.u. for CBFO (undoped). In CBFO, both Fe^{2+} and Fe^{3+} are located in tetrahedral sites and consequently are both in high spin configuration $e_g^3t_{2g}^3(\mu_{\text{eff}}=9.8\mu_B)$ for Fe^{2+} and $e_g^2t_{2g}^3(\mu_{\text{eff}}=11.8\mu_B)$ for Fe^{3+}. The analysis of the structure indicated that there exist two sites for iron cations: 75% is located in kagome layers (Fe2 site) and 25% site in the triangular layers (Fe1 site).[13] Consequently, it is most probable that these oxides are ferrimagnetic, with the iron cations showing a ferromagnetic component in each sublattice (kagome and triangular). Considering an AFM coupling between Fe^{2+}/Fe^{3+} sublattices, the FiM interaction could result from the noncompensation of the sublattice magnetizations. From the charge balance "$2Fe^{2+}$:$2Fe^{3+}$" in $CaBaFe_4O_7$, a quantum mechanical spin μ_{eff} of $10.8\mu_B$ per f.u. could be expected ($\mu_{\text{eff}}=[2\times5.9^2+2\times4.9^2]^{1/2}$), whereas, CBFO exhibits lesser magnetic moment of $3.2\mu_B$/f.u.. As x increased in $CBFLi_x$ series, the μ_{eff} shows a monotonic increases from 3.75 ($x=0.1$) to $5.55\mu_B$/f.u. ($x=0.4$). However, all the $CBFLi_x$ samples indicate a reduced μ_{eff} value compared to the theoretically estimated one, which is reminiscent of geometrically frustrated systems.

C. Magnetic-field variation in magnetization $M(H)$

In view of the present observations on the irreversibility of $M_{\text{FC}}(T)$ and $M_{\text{ZFC}}(T)$ curves at lower temperatures, detailed investigations were performed on the isothermal field driven dc magnetization $M(H)$ curves at four different temperatures. Figures 3(a)–3(d) show the $M(H)$ curves recorded at temperatures of 5, 50, 100, and 250 K, respectively. For CBFO, one observes a large hysteresis loop of H_C ~0.75 T much larger than the magnetic field used for M_{FC}-M_{ZFC} measurements [Fig. 3(a)]. There is a marginal increase in H_C to ~1.24 T for $CBFLi_{0.1}$ and ~1.17 T for $CBFLi_{0.2}$ at 5 K. The particular shape of the loop for CBFO at 5 K, involving a steplike behavior at 0.4 T, can be explained by a strong pinning of the domain walls [Fig. 3(a)].

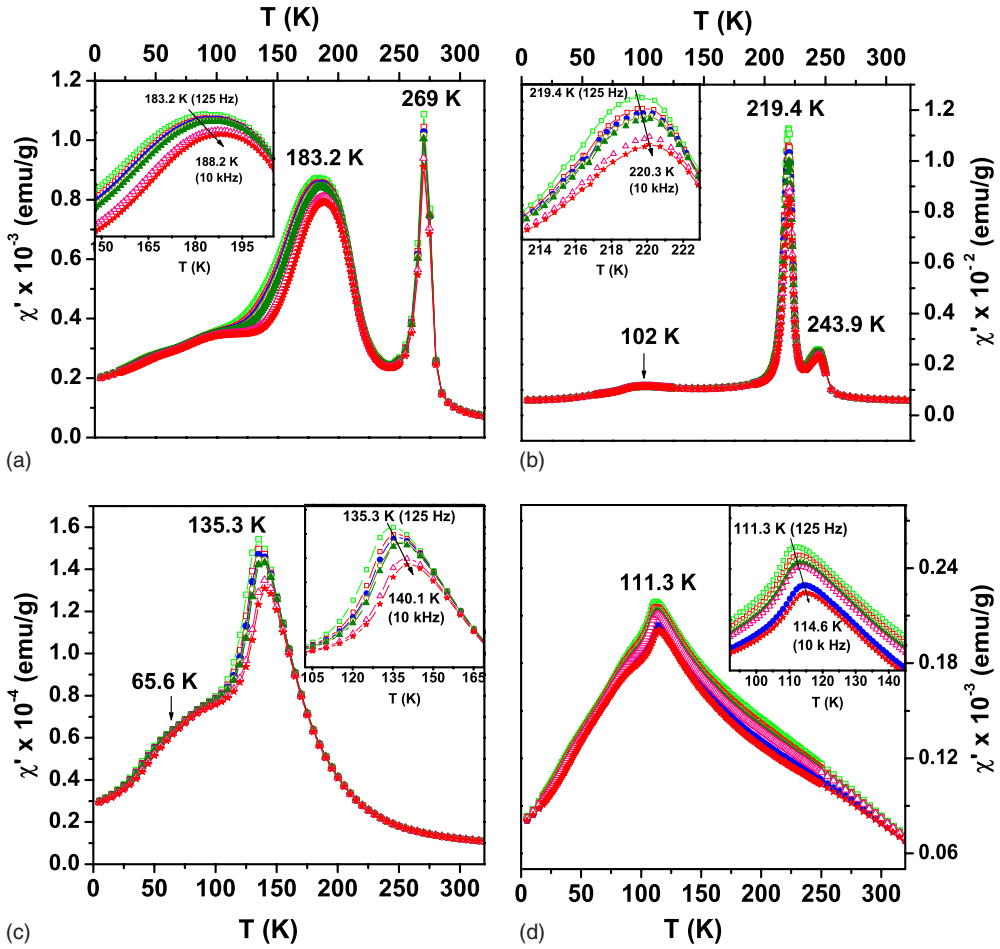

FIG. 4. (Color online) The real (in-phase) χ'_{ac} component of ac susceptibilities for (a) $CaBaFe_4O_7$ (b) $CBFLi_{0.1}$ (c) $CBFLi_{0.3}$, and (d) $CBFLi_{0.4}$ as a function of temperature at the frequency $f=125$ Hz–10 kHz at zero static magnetic field (H_{dc}), and at a driving ac fields (H_{ac}) of 10 Oe. The arrows indicate the location of peaks at $f=125$ Hz. Inset: The magnification of the transition at the freezing temperature (T_f). The measuring frequencies (in Hz) are: 125 (■), 325 (□), 525 (●), 725 (○), 1000 (▲), 5000 (△), and 10 000 (*).

The saturation magnetization ($\mu_{H,5\ K}$) at 5 K indicates only a marginal decrease from 2.6 (for CBFO) to $\sim 1.15\mu_B$/f.u. for $CBFLi_{0.3}$. For all the samples, the $\mu_{H,100\ K}$ marginally decreases from that of $\mu_{H,5\ K}$ (Table II). The $M(H)$ curves collected below FiM-PM transition (T_C) clearly show a lack of magnetic saturation even under the magnetic field of 5 T. Hence, the saturation magnetization (μ_H) was determined at the ordinate point intercepted by the extrapolation from the linear high-field region of $M(H)$ curve. This criterion eliminates the linear nonsaturating behavior, which is increasingly visible for all the samples of $CBFLi_x$ [Figs. 3(b)–3(d)]. The higher values of H_C's indicate that $CaBaFe_{4-x}Li_xO_7$ series is a hard ferrimagnet. The μ_H decreases with increasing temperature as well as the Li content in $CBFLi_x$ [Figs. 3(b)–3(d)]. Similarly, the coercive field (H_C) also decreases progressively, and finally above T_C, the $M(H)$ behavior becomes linear, indicative of the paramagnetic behavior at high temperature. The large H_C's and the nonattainment of saturation of $M(H)$ curves even at field up to 5 T could be corroborated with that of the dc-$M_{FC}(T)$ curves. This behavior further strengthens the fact that the growing presence of canted-AFM clusters or competing spin interactions could prevail in these 114 ferrites.

D. ac magnetic susceptibility study

1. Real part versus temperature, $\chi'_{ac}(T)$

The measurements of the ac magnetic susceptibility $\chi'_{ac}(T,f)$ were made in zero dc magnetic field ($H_{dc}=0$) between 5 to 320 K and at the frequency (f) ranging from 10 to 10 000 Hz using the PPMS. The amplitude of the ac magnetic field was $H_{ac}\sim 10$ Oe. The real part (in-phase) component of the magnetic susceptibility, $\chi'_{ac}(T)$ for all $CBFLi_x$ series is plotted in Fig. 4. The $\chi'_{ac}(T)$ curves of undoped CBFO indicate a broader transition at the freezing temperature (T_f) at around ~183 K when compared to that of $CBFLi_x$ samples [Fig. 4(a)]. For $CBFLi_x$ series, the $\chi'_{ac}(T)$ curves exhibit a maximum at T_f which is much below the FiM-PM transition temperature (T_C) estimated from that of the M_{FC} curves of DCM measurements (Table III). Below the freezing temperature, the temperature dependence of χ'_{ac} varies differently with every compound. For $CBFLi_{0.1}$, the $\chi'_{ac}(T)$ curves exhibit a sharp transition near the freezing temperature (T_f) of about 219.4 K (at 125 Hz) associated with small cusps at around ~243.9 and 102 K, respectively. However, these cusps are also frequency dependent. With further increase of $x\sim 0.2$ (not shown in Fig. 4), the shoulder cusp

TABLE III. The magnetic properties extracted from the ac magnetic susceptibility data.

Sample	T_C (K)	T_{max} from $\chi'(T)$ (K)	T_{max} from $\chi''(T)$ (K)	Spin-relaxation time τ_o (s)	$z\nu$	Activation energy (average) E_a (eV)	Spin-glass transition temperature T_g (K)
0	265.6	183.2	165.1	4.9×10^{-12}	6.4	0.019	176
0.1	221.2	219.4	218	1.28×10^{-14}	13.2	0.065	127.2
0.2	191.6	188.2	176.5	4.4×10^{-14}	12.8	0.08	122.5
0.3	150.7	140.5	125.5	2.4×10^{-15}	13.8	0.094	117.4
0.4	97.5	111.1	108	8.1×10^{-16}	12.6	0.11	101.8

on $\chi'_{ac}(T)$ curve is restored, the shape of the function of $\chi'_{ac}(T,f)$ similar to that of $CBFLi_{0.1}$ sample [Fig. 4(b)], showing about 40 K lower T_f (~172 K at 125 Hz) values and a lower absolute value of χ'_{ac}. As is evident from Figs. 4(c) and 4(d), the behavior of $\chi'_{ac}(T,f)$ for $CBFLi_{0.3}$ is similar to that of $CBFLi_{0.1}$ except for the broader transition at T_f. However, a shoulder peak is not observed for $CBFLi_{0.3}$ and an almost monotonous increase in χ'_{ac} values appears associated with the onset of frequency dependent $\chi'_{ac}(T)$. In contrast, $CBFLi_{0.4}$ exhibits a unique χ'_{ac} transition at ~111 K, characterized by a broad maximum [Fig. 4(d)]. Below this transition, there is only a linear decrease in χ'_{ac} values with temperature without any anomaly or hump. The Li^{1+} substitution plays a dominant role not only in magnitude of χ'_{ac} near T_f but also in the sharpness and form of the χ'_{ac} curves around T_f. Nevertheless, the sharp maximum in χ'_{ac} at around 269 K for CBFO is independent of frequency indicating that it is not related to spin-glass transition [Fig. 4(a)]. Upon examining the insets of Figs. 4(a)–4(d), it is also possible to conclude that $CBFLi_x$ series exhibits frequency-dependent T_f values; i.e., as the frequency (f) is increased, the T_f shifts to higher values associated with the decrease in the magnitude of χ'_{ac}. For CBFO, the T_f value of 183.2 K (at 125 Hz) increases to ~188.2 K (at 10 KHz). But with further decrease in temperature below T_f, the frequency dependence of χ'_{ac} vanishes. This behavior is the same for all Li-substituted $CBFLi_x$ samples and strongly suggests a spin glass or superparamagnetic behavior, which will be treated accordingly in the discussion below.

2. *Imaginary part versus temperature,* $\chi''_{ac}(T)$

In the same way as for the imaginary component (out of phase) of ac susceptibility, there exists an obvious scaling difference in the χ''_{ac} plots shown as a function of temperature (Fig. 5). The relative-energy losses during the magnetic transition at $T_f(\chi'/\chi'')$ vary from 7.2, 19, 8.2, and 4.3% for x ranging from 0 to 0.4. For all $CBFLi_x$ samples, the energy loss at the freezing temperature is significant, suggesting that the transitions themselves are nonspontaneous. For all $CBFLi_x$ ($0\leq x\leq 0.4$) samples, the maximum in the $\chi''_{ac}(T)$ curves [Figs. 5(a)–5(d)] appears just below the maximum of $\chi'_{ac}(T)$ curve [Figs. 4(a)–4(d)] and is also frequency dependent. However, the difference in temperature between the T_f values in χ'_{ac} and χ''_{ac} changes significantly with the lithium content. As an example, $T_f(\chi'_{ac})-T_f(\chi''_{ac})$ values at 125 Hz are 18, 1.4, 3.2, 15, and 3.1 K for $x=0$, 0.1, 0.2, 0.3, and 0.4, respectively. This irregular variation in the difference is not understood. In fact, the number of magnetic-relaxation peaks increases with the lithium concentration [Figs. 5(b)–5(d)]. The $CBFLi_{0.4}$ sample exhibits a broad maximum at ~210 K associated with a sharp maximum at ~108 K and followed by a small rounded hump at ~42 K (at 125 Hz) [Fig. 5(d)]. Samples with higher Li content ($CBFLi_{0.3}$ and $CBFLi_{0.4}$) showed a second maximum or a shoulder peak on the low-temperature side of $\chi''_{ac}(T)$ curve. Bearing in mind that the samples $CBFLi_x$ with $x=0.3$ and 0.4 are really monophasic, they might exhibit a secondary redistribution of magnetic spins at around 49 and 45 K, respectively. As underlined by Mydosh,[20] a spin-glass (SG) transition is characterized by other signatures which are less often investigated. For instance, for spin glasses, the temperature of the peak in χ'_{ac} must correspond to the inflection point on the high-temperature side of the $\chi''_{ac}(T)$ maximum.[21,22] Figure 5(c) shows the enlargements of χ'_{ac} and χ''_{ac} curves for $CBFLi_{0.3}$ in the region of the peak maxima (T_f). In the $\chi'_{ac}(T)$ data, the location of the maximum of $\chi'_{ac}(T)$ is found to be consistent with the midpoint of the increase in $\chi''_{ac}(T)$ for decreasing temperature, another result which supports the SG nature of the transition [Fig. 5(c)].

The conclusions based on the qualitative features of ZFC and field-cooled dc magnetic susceptibilities are: first, the ZFC $\chi_{dc}(T)$ curve exhibits a peak; second, the M_{FC} and M_{ZFC} curves diverge from each other below the temperature of this peak. The dc magnetization measurements show the typical behavior for paramagnetic materials at higher temperatures ($T\gg T_f$) as evidenced by Curie-Weiss plots. Further, there exist no saturation in $M(H)$ and coercive fields are very large. We have already specified that this behavior is one of the hallmarks of SG behavior.[23] Considering the χ'_{ac} and χ''_{ac} curves, one observes that the location of the peak in $\chi'(T)$ is shifted to higher T as the frequency is increased, while the magnitude of $\chi'(T)$ is decreased. It must be emphasized that this is precisely the behavior expected for a spin-glass transition.[24] As already noticed, the presence of a peak in $\chi'(T)$ is indicative of a spin-glass behavior, but it is not a proof in itself. Moreover, the estimated transitions, where the M_{ZFC} curve starts to deviate significantly from that of the M_{FC} curve (T_r), are about ~183, 201, 185, 128, and 112 K for $CBFLi_x$ with $0\leq x\leq 0.4$, respectively. These values are nearly comparable with that of the T_f values observed from the $\chi'_{ac}(T)$ measurements. The fact that the bifurcation be-

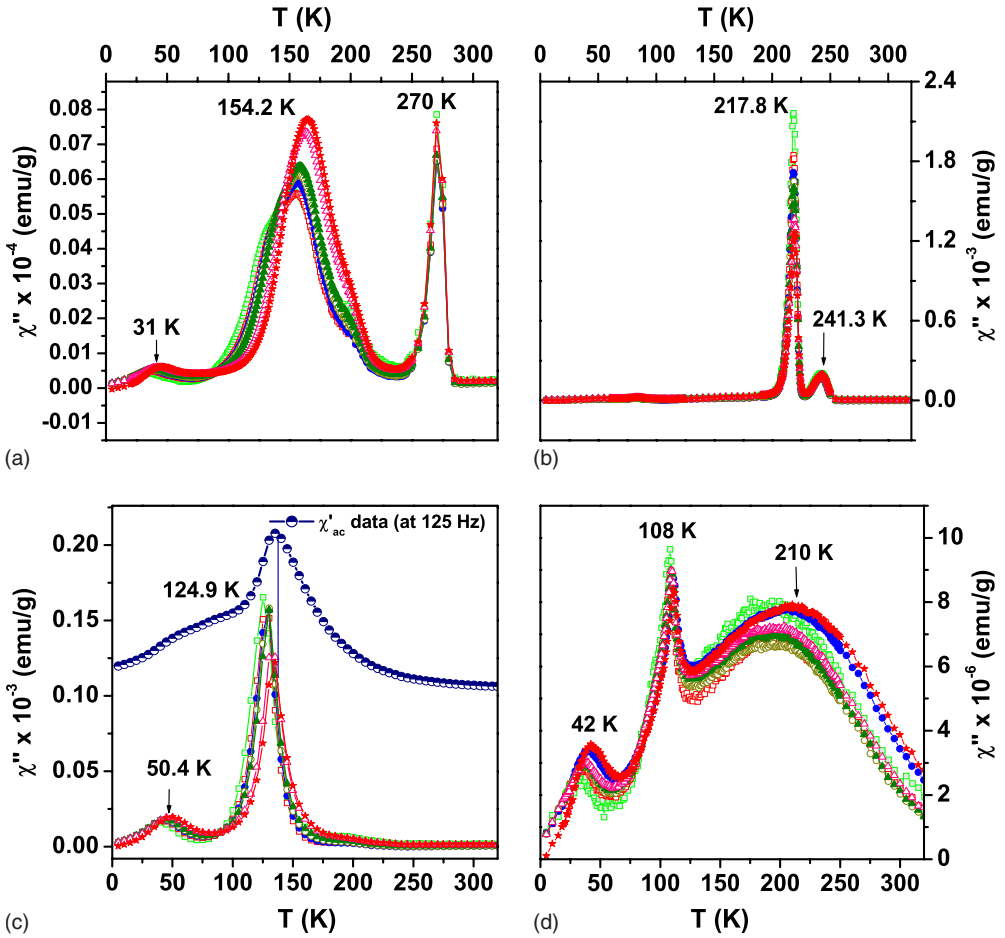

FIG. 5. (Color online) The imaginary (out of phase) χ''_{ac} component of ac susceptibilities for (a) $CaBaFe_4O_7$ (b) $CBFLi_{0.1}$ (c) $CBFLi_{0.3}$, and (d) $CBFLi_{0.4}$ as a function of temperature at the frequency $f=125$ Hz–10 KHz at zero static magnetic field (H_{dc}), and at a driving ac fields (H_{ac}) of 10 Oe. The arrows indicates the location of peaks at $f=125$ Hz. The measuring frequencies (in Hz) are: 125 (■), 325 (□), 525 (●), 725 (○), 1000 (▲), 5000 (△), and 10 000 (*).

tween M_{FC} and M_{ZFC} curve starts deviating much above T_f, as detected by the dynamic magnetic measurements, is in favor of a spin-glass state whose spins tend to freeze slowly over a larger temperature range. Furthermore, we also emphasize the contributions by the domain wall pinning effect to the magnetic relaxations observed in imaginary component of ac susceptibility (χ''_{ac}) wherein the pinned domain walls can be thermally activated at higher temperatures. Hence, the magnetic susceptibility can increase slowly leading to a magnetic-relaxation peak which occurs at the temperature where the domain wall pinnings are overcome.

To check the existence of a spin-glass behavior in $CaBaFe_{4-x}Li_xO_7$ samples, we have analyzed the frequency dependence of maxima in $\chi'_{ac}(T)$ for undoped CBFO sample and one of $CBFLi_x$ series, having higher x value that yields a pure compound, $CBFLi_{0.4}$. This characteristic temperature is most often associated with the location of the peak in $\chi'(T)$. However, the frequency dependence of a freezing temperature (T_f) can be tracked by considering the location of the peak maxima in $\chi'_{ac}(T)$, which allows us to get a better resolution owing to the larger amplitude of the signal. Doing so in the case of $CBFLi_{0.4}$, we can follow the frequency dependence of T_f over three decades. The nature of the temperature and frequency dependences of T_f in a genuine SG has been the subject of intense debate in the last decades. However, the dynamic scaling theory[24] is generally admitted to be the most relevant to account for a spin-glass transition.[25] This theory predicts a power law of the form $\tau=\tau_0(T_f-T_{SG}/T_{SG})^{-z\nu}$, where τ_0 is the shortest relaxation time available to the system, T_{SG} is underlying spin-glass transition temperature determined by the interactions in the system, z is the dynamic critical exponent, and ν is the critical exponent of the correlation length. A good test for the relevance of the power-law model consists of using the equivalent form as

$$\ln(\tau)=\ln(\tau_0)-z\nu\log\left(\frac{T_f-T_{SG}}{T_{SG}}\right). \quad (1)$$

We proceeded as follows: (i) first, the value of spin-glass transition temperature, T_{SG}, was adjusted in order to get the best linearity in the $\ln(\tau)$ versus T_f plots; (ii) then, the spin-relaxation time, τ_0, and the dynamic critical exponents, $z\nu$, were derived from the parameters of the linear fitting. The values of parameter that showed the best fitting for Eq. (1) are given in Fig. 6 (inset). From Figs. 6(a) and 6(b), one observes the existence of a remarkable linearity over three

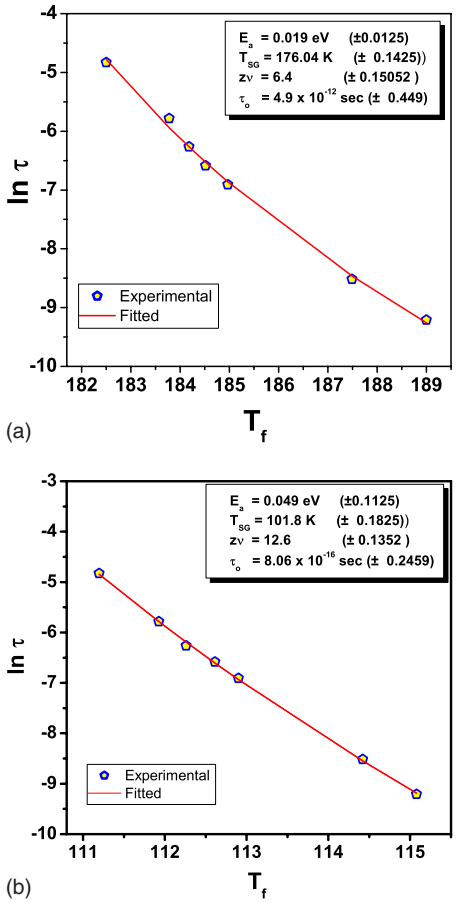

FIG. 6. (Color online) Plot of $\ln(\tau)$ versus freezing temperature (T_f) for (a) $CaBaFe_4O_7$ and (b)$CBFLi_{0.4}$ characteristic of the power-law model (see text). The figure displays the best fitting that corresponds to the following values of parameters that are shown in the inset of the corresponding figures.

decades, which shows that the spin-glass transition in CBFO and $CBFLi_x$ well obeys the behavior expected for SG's. The values of best fitting parameters obtained for undoped CBFO are as follows: $T_{SG}=176$ K, $\tau_0=4.9\times10^{-12}$ s, and $zv=6.4$ (Table III). As expected in the dynamic scaling theory, the value of T_{SG} is close to the location of the maximum in the M_{ZFC} curves. One can also notice that τ_0 lies within the range of values typical of spin glasses ($10^{-10}-10^{-12}$ s).[26] As for zv, it is well within the values expected for canonical spin glasses ($zv=5-10$).[27,28] The spin-relaxation time is also in range of SG's and it remains consistent with the results of other types of spin glasses, such as $Ho_5Co_{50}Al_{45}$ (Ref. 29) and $La_{1-x}Ca_xMnO_3$ ($0\leq x\leq0.15$).[30] Furthermore, the parameters that we obtained for CBFO by fitting with the Vogel-Fulcher law, $\tau=\tau_o\exp[E_a/k_B(T_f-T_{SG})]$,[26] have reasonable comparison with those obtained from power law following Eq. (1). On the other hand, for $CBFLi_x$ samples, the $\ln\tau$ versus freezing temperature (T_f) also gives an excellent linear dependence [as shown in Fig. 6(b)]. The best fitting parameters are: $\tau_0=1.28\times10^{-14}$ s, $zv=13.2\pm2$, and $T_{SG}=127\pm3$ K for $CBFLi_{0.1}$ whereas for sample $CBFLi_{0.4}$, $\tau_0=8.1\times10^{-16}$ s, $zv=12.6\pm2$, and $T_{SG}=101\pm3$ K. The glass transition temperature T_{SG} decreased with increasing Li content. The activation energy, ΔE_a, (average) is ~0.065 (2) eV for $CBFLi_{0.1}$ and indicates a marginal increase to 0.08 eV for $CBFLi_{0.2}$ and to 0.11 eV for $CBFLi_{0.4}$. Furthermore, these values are also slightly different from those extracted using the Vogel-Fulcher law. The spin-relaxation time (τ_0) for $CBFLi_x$ series decreases drastically from that of undoped CBFO. In fact, the estimated values of critical exponents zv and τ_0 are not consistent with those values reported for the spin glasses and lie much closer to that of cluser glasses ($\tau_0=10^{-14}-10^{-16}$ s; $zv=12-14$).[24] Moreover, the increased τ_0 values indicate that there is a clear size distribution in the spin clusters. This is further corroborated by the increased number of magnetic-relaxation peaks and the broader transition with increasing Li content for $CBFLi_x$ [Figs. 5(b)–5(d)]. To summarize, the power-law model [Eq. (1)] provides a satisfactory description of our T_f (f) data of $CBFLi_x$ for $0.1\leq x\leq0.4$, demonstrating a critical slowing down model typical for spin clusters. Hence, a clear transition from spin-glasses behavior (for CBFO) to cluster glass (for $CBFLi_x$) is evident from the analysis of dynamic magnetic susceptibility (χ'_{ac} and χ''_{ac}) measurements. Such behavior can possibly arise from (i) the presence of competing (SE and FiM) interactions or (ii) the existence of randomness in the spatial distribution of these interactions due to substitutional effects.[11,12] The Li^{1+} cation can substitute in both Fe^{2+} and Fe^{3+} sites, i.e., at the kagome layers or at the triangular layers (between the kagome layers). Consequently, the substitution can cut the magnetic interactions between the kagome layers, introducing a disorder in Fe^{2+}-Li^{1+}-Fe^{3+} exchange couplings. Hence, it can disrupt the localized FiM ordering both at the kagome and the triangular layers. Several authors reported the coexistence of two or more spatially separated magnetic phases which is, in turn, induced at different concentration levels of magnetic impurities: (i) spin glass to ferromagnetism in $CdCr_{2x}In_{2-2x}S_4$ (Ref. 31) and $La_{0.5}Sr_{0.5}CoO_3$,[32] (ii) spin glass to antiferromagnetism in $Fe_xZn_{1-x}F_2$ (Ref. 33) or (iii) spin glass to superconductivity in $La_{2-x}Sr_xCuO_4$.[34] Presently, the spin glass to spin cluster transition behavior of these substituted 114 ferrites are found to be delicate since it often corresponds to a situations lying at the borderline between the itinerant and localized pictures.

E. Transport properties: analysis of temperature variation in resistivity $\rho(T)$ curves

The evolution of the resistivity versus temperature of the $CaBaFe_{4-x}Li_xO_7$ samples [Fig. 7(a)] shows that all these oxides are semiconductors and that the resistivity increases with the lithium content. Moreover, no resistivity transition or anomaly could be detected in contrast to $LnBaCo_4O_7$. Thus, the iron ferrites differ significantly from the cobaltites which exhibits a step in the $\rho(T)$ curves due to a structural transition associated with the release of magnetic frustration. The resistivity measurements under $H=7$ T show that the $CBFLi_x$ samples do not exhibit any magnetoresistance except the undoped phase CBFO [Fig. 7(b)]. The latter shows a magnetoresistance, maximum at 264 K, MR ~4.3%, which indicates a possible charge localization.

The analysis of $\rho(T)$ data was carried out considering the following models:[35,36] Arrhenius, small polaronic hopping

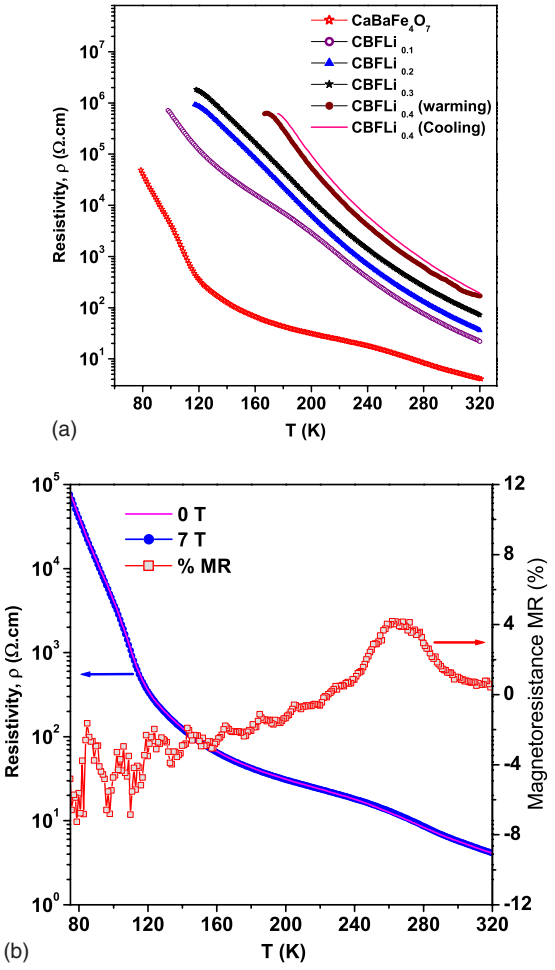

FIG. 7. (Color online) (a) Temperature-dependent electrical resistivity $\rho(T)$, for $CBFLi_x$ $(0 \leq x \leq 0.4)$. The arrows indicate the $\rho(T)$ curves of $CBFLi_{0.4}$ during heating (–△–) and cooling (—) cycles. (b) The resistivity $\rho(H,T)$ in an applied magnetic field of $H=0-7$ T for undoped CBFO.

(SPH), Efros–Shklovskii-type hopping (ESH), and Mott's 3D variable range hopping (VRH) model. To check for the validity of the above-mentioned models, the log ρ were fitted as a function of T^n, where $n=-1,-1/2$ or $-1/4$ (Fig. 8). The $\rho(T)$ data provided a significant nonlinearity when fitted with Arrhenius model, indicating that a simple thermal activation of charge carriers alone does not account for the charge transport. Furthermore, plotting the $\rho(T)$ according to ESH model did not give a straight line either. In contrast, at temperature ≥ 200 K, $\rho(T)$ data could be fitted with adiabatic SPH conductivity. Thus, from the nearly linear region of Fig. 8, the activation energy (E_a) and resistivity coefficient (B) have been calculated from the formula, $BT\exp(E_a/k_BT)$ for each sample. The ΔE_a (average) ranges from 0.11 eV for $x=0.1$ to 0.18 eV for $x=0.4$, whereas, the resistivity coefficient (B) varies between 2.8 and 1.5×10^{-6} Ω cm/K. This implies that unlike a band-gap semiconductor, the temperature-dependent quantity is the mobility and not the carrier concentration. However, the low-temperature $\rho(T)$ data are better described by VRH model $[\rho=\rho_o\exp(T_o/T)^{-1/4}]$, which, in turn, indicates a possible

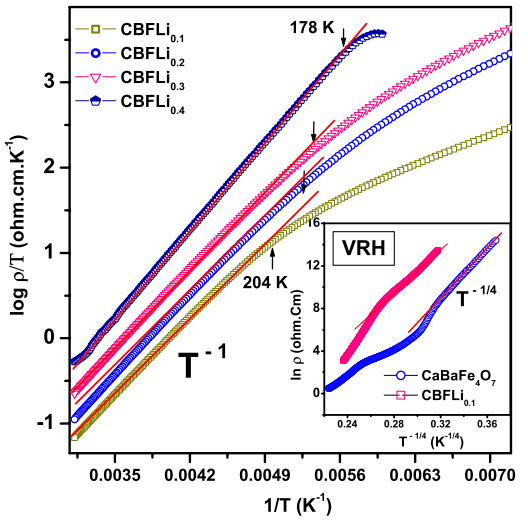

FIG. 8. (Color online) Logarithm of resistivity $\log(\rho/T)$ versus T^{-n} plots (where $n=1$ or $\frac{1}{4}$) for $CaBaFe_{4-x}Li_xO_7$. Open symbols and solid lines represent the experimental data and linear fit to the different hopping models as described in the text.

crossover to different conduction mechanisms at low temperatures. The fit to $\rho_o\exp(T_o/T)^{-1/4}$ gives T_o (interpreted as E_a in the SPH model) in the range of ~1139 to 1356 K for $CBFLi_y$ samples. The temperature of deviation from SPH model (indicated by arrows in Fig. 8) increases with Li content. Thus these oxides exhibit very complicated charge transport properties which cannot satisfy unique conduction model for the entire temperature regime.

IV. CONCLUSIONS

The study of the 114 $CaBaFe_{4-x}Li_xO_7$ oxides shows that in spite of their structural similarity with 114 cobaltites, their magnetic and transport properties are very different. These oxides can be described as frustrated ferrimagnets whose T_c decreases dramatically as the lithium content increases. Moreover, these compounds are hard ferrimagnets with high-coercive fields ranging from 0.7 to 0.9 T. Importantly, the ac magnetic susceptibility measurements show that $CaBaFe_4O_7$ is a typical spin glass. In contrast, for the Li-substituted oxides, the broad appearance of the spin-freezing transition temperature as observed from the ac susceptibility measurements $\chi'_{ac}(T)$ and the multiple relaxation peaks in imaginary component of $\chi''_{ac}(T)$ curves are not indications of spin glasses but rather of a spin-cluster behavior. The $CBFLi_y$ samples presented here contain a spin-glass feature together with a second-magnetic feature, of which a disordered antiferromagnet or a spin-cluster formation is possible. Thus, the magnetic properties of $CaBaFe_{4-x}Li_xO_7$ series as a whole can be described as changing from spin glass to cluster glass as x increases. These results open the route to the investigation of the substitutional effect of other magnetic and nonmagnetic cations for iron in the $CaBaFe_4O_7$ oxide upon the magnetic properties of these materials.

*FAX: (33)231951600; bernard.raveau@ensicaen.fr

[1] J. E. Greedan, J. Alloys Compd. **444**, 408 (2006).
[2] Y. Muraoka, H. Tabata, and T. Kawai, J. Appl. Phys. **88**, 7223 (2000).
[3] G. E. Delgado, V. Sagredo, and F. Bolzoni, Cryst. Res. Technol. **43**, 141 (2008).
[4] M. Valldor, Solid State Sci. **6**, 251 (2004).
[5] M. Valldor and A. Anderson, Solid State Sci. **4**, 923 (2002).
[6] N. Nakayama, T. Mizota, Y. Ueda, A. N. Sokolov, and A. N. N. Vasiliev, J. Magn. Magn. Mater. **300**, 98 (2006).
[7] A. Huq, J. F. Mitchell, H. Zheng, L. C. Chapon, P. G. Radaelli, K. S. Knight, and P. W. Stephens, J. Solid State Chem. **179**, 1136 (2006).
[8] V. Caignaert, A. Maignan, V. Pralong, S. Hebert, and D. Pelloquin, Solid State Sci. **8**, 1160 (2006).
[9] A. Maignan, C. Martin, D. Pelloquin, N. Nguyen, and B. Raveau, J. Solid State Chem. **142**, 247 (1999).
[10] L. C. Chapon, P. G. Radaelli, H. Zheng, and J. F. Mitchell, Phys. Rev. B **74**, 172401 (2006).
[11] M. Valldor, Solid State Sci. **6**, 251 (2004); M. J. Valldor, J. Phys.: Condens. Matter, **16**, 9209 (2004); M. Valldor, J. Phys. Chem. Solids **66**, 1025 (2005).
[12] A. Maignan, J. Solid State Chem. **181**, 1220 (2008).
[13] B. Raveau, V. Caignaert, V. Pralong, D. Pelloquin, and A. Maignan, Chem. Mater. **20**(20), 6295 (2008).
[14] V. Caignaert, A. M. Abakumov, D. Pelloquin, V. Pralong, A. Maignan, G. Van Tendeloo, and B. Raveau, Chem. Mater **21**, 1116 (2009).
[15] J. Rodriguez-Carvajal, An Introduction to the Program FULLPROF 2000; Laboratoire Léon Brillouin, CEA-CNRS: Saclay, France, (2001).
[16] R. D. Shannon and C. T. Prewitt, Acta Crystallogr., Sect. B: Struct. Crystallogr. Cryst. **25**, 925 (1969).
[17] R. F. Wang, J. Li, W. M. Nisoli, X. Ke, J. W. Freeland, V. Rose, M. Grimsditch, P. Lammert, V. H. Crespi, and P. Schiffer, J. Appl. Phys. **101**, 09J104 (2007).
[18] R. Roy and S. Das, J. Appl. Phys. **104**, 103915 (2008).
[19] A. Maignan, C. Martin, F. Damay, and B. Raveau, Phys. Rev. B **58**, 2758 (1998).
[20] A. J. Mydosh, *Spin Glasses: An Experimental Introduction* (Taylor and Francis, London, 1993).
[21] D. Huser, L. E. Wenger, A. J. van Duyneveldt, and J. A. Mydosh, Phys. Rev. B **27**, 3100 (1983).
[22] I. R. Fisher, K. O. Cheon, A. F. Panchula, P. C. Canfield, M. Chernikov, H. R. Ott, and K. Dennis, Phys. Rev. B **59**, 308 (1999).
[23] I. G. Deac, J. F. Mitchell, and P. Schiffer, Phys. Rev. B **63**, 172408 (2001).
[24] P. C. Hohenberg and B. I. Halperin, Rev. Mod. Phys. **49**, 435 (1977).
[25] J. Souletie and J. L. Tholence, Phys. Rev. B **32**, 516 (1985).
[26] K. Gunnarsson, P. Svedlindh, P. Nordblad, L. Lundgren, H. Aruga, and A. Ito, Phys. Rev. Lett. **61**, 754 (1988).
[27] J. Souletie and J. L. Tholence, Phys. Rev. B **32**, 516 (1985).
[28] K. H. Fischer and J. Hertz, *Spin Glasses* (Cambridge University Press, Cambridge, 1991).
[29] J. L. Tholence, Physica B (Amsterdam) **126**, 157 (1984).
[30] R. Laiho, E. Lähderanta, J. Salminen, K. G. Lisunov, and V. S. Zakhvalinskii, Phys. Rev. B **63**, 094405 (2001).
[31] S. Viticoli, D. Fiorani, M. Nogues, and J. L. Dormann, Phys. Rev. B **26**, 6085 (1982).
[32] D. N. H. Nam, K. Jonason, P. Nordblad, N. V. Khiem, and N. X. Phuc, Phys. Rev. B **59**, 4189 (1999).
[33] D. P. Belanger, Wm. E. Murray, F. C. Montenegro, A. R. King, V. Jaccarino, and R. W. Erwin, Phys. Rev. B **44**, 2161 (1991).
[34] S. Wakimoto, S. Ueki, Y. Endoh, and K. Yamada, Phys. Rev. B **62**, 3547 (2000).
[35] N. F. Mott, J. Non-Cryst. Solids **1** (1968); A. L. Efros and B. I. Shklovskii, J. Phys. C **8**, L49 (1975).
[36] A. K. Sen and S. Bhattacharya, arXiv:cond-mat/0506089 (unpublished).